

Neural Implicit Mapping via Nested Neighborhoods

Vinicius da Silva
PUC-Rio

Tiago Novello
IMPA

Guilherme Schardong
U Coimbra

Luiz Schirmer
U Coimbra

Helio Lopes
PUC-Rio

Luiz Velho
IMPA

Abstract

We introduce a novel approach for rendering **static and dynamic** 3D neural signed distance functions (SDF) in real-time. We rely on nested neighborhoods of zero-level sets of neural SDFs, and mappings between them. This framework **supports animations** and achieves real-time performance **without the use of spatial data-structures**. It consists of three uncoupled algorithms representing the rendering steps. The **multiscale sphere tracing** focuses on minimizing iteration time by using coarse approximations on earlier iterations. The **neural normal mapping** transfers details from a fine neural SDF to a surface nested on a neighborhood of its zero-level set. It is smooth and it does not depend on surface parametrizations. As a result, it can be used to **fetch smooth normals for discrete surfaces** such as meshes and to skip later iterations when sphere tracing level sets. Finally, we propose an algorithm for **analytic normal calculation for MLPs** and describe ways to obtain sequences of neural SDFs to use with the algorithms.

1. Introduction

Neural signed distance functions (SDF) emerged as an important model representation in computer graphics. They are neural networks representing SDF of surfaces, which can be rendered by finding their zero-level sets. The *sphere tracing* (ST) [12, 13] is the standard algorithm for this task.

Neural SDFs created new paths of research challenges, including how to render their level sets flexibly and efficiently. In this work, we approach the problem of *real-time rendering* of neural SDFs level sets. Previous approaches train specific spatial data-structures, which may be restrictive for dynamic models. Another option is to extract the level sets using marching cubes, which needs precomputation, results in meshes that require substantially more storage than neural SDFs, and depends on grid resolution.

We propose a novel framework for real-time rendering of neural SDFs based on *nested neighborhoods* and mappings between them. It supports animations and achieves real-time performance without the use of spatial data-structures.

We define three algorithms to be used with such neural SDFs. The *multiscale ST* uses the nested neighborhoods to minimize the overhead of iterations, relying on coarse versions of the SDF for acceleration.

Given a coarse surface S nested in a neighborhood of the zero-level set of a detailed neural SDF, the *neural normal mapping* transfers the detailed normals of the level sets to S . This procedure is smooth and is very appropriate to transfer details during the rendering because it does not depend on parametrizations. As a result, it can be used to fetch smooth normals for discrete surfaces such as meshes and to skip later iterations when sphere tracing level sets.

Finally, we propose an algorithm for analytic normal calculation for MLPs and describe ways to obtain sequences of neural SDFs to use with the algorithms. Summarizing, the contributions of this framework are the following:

- Real-time rendering of static and animated 3D neural SDFs without spatial data-structures;
- Multiscale ST to minimize ST iteration overhead;
- Neural normal mapping to transfer the level set normals of a finer neural SDF to the level sets of a coarser SDF or to a discrete surface;
- Analytic normal calculation for MLPs to compute smooth normals;
- Methods to build sequences of neural SDFs with the neighborhoods of their zero-level sets nested.

2. Related Work

Implicit functions are an essential topic in computer graphics [28]. SDFs are important examples of such functions [3] and arise from solving the Eikonal problem [25]. Recently, neural networks have been used to represent SDFs [11, 23, 26]. *Sinusoidal networks* are an important example, which are *multilayer perceptrons* (MLPs) having the sine as its activation function. We use the framework in [22] to train the networks which consider the parameter initialization given in [26].

Marching cubes [15, 19] and *sphere tracing* [12, 13] are classical visualization methods for rendering SDF level sets. Neural versions of those algorithms can also be found in [4, 16, 18]. While the initial works in neural SDFs use marching cubes to generate visualizations of the resulting level sets [11, 23, 26], recent ones have been focusing on sphere tracing, since no intermediary representation is needed for rendering [8, 27]. We take the same path.

Fast inference is needed to sphere trace neural SDFs. Davies et al. [8] shows that this is possible using General Matrix Multiply (GEMM) [9, 21], but the capacity of the networks used there does not seem to represent geometric detail. Instead, we use the neural SDF framework in [22] to represent detailed geometry. Our approach is to show that ST can be adapted to handle multiple neural SDFs and that we can transfer details from them during the process. We also compute the analytic neural SDF gradients to improve shading performance and accuracy during rendering.

State-of-the-art works in neural SDFs store features in the nodes of *octrees* [20, 27], or limit the frequency band in training [17]. Octree-based approaches cannot directly handle dynamic models. On the other hand, our method does not need spatial data structures, supports animated surfaces, and provides smooth normals which are desired during shading.

Normal mapping [5, 6] is a classic method to transfer detailed normals between meshes, inspired by *bump mapping* [2] and *displacement mapping* [14]. Besides depending on interpolation, normal mapping also suffers distortions of the parametrization between the underlying meshes, which are assumed to have the same topology. Using the continuous properties of neural SDFs allows us to map the gradient of a finer neural SDF to a coarser one. This mapping considers a volumetric neighborhood of the coarse surface instead of parametrizations and does not rely on interpolations like the classic one.

3. Nested Neighborhoods of neural SDFs

This section describes our method. The objective is to render level sets of neural SDFs in real-time and in a flexible way. Given the iterative nature of the ST, a reasonable way to increase its performance is to optimize each iteration or avoid them. The key idea is to consider neural SDFs with a small number of parameters as an approximation of earlier iterations and map the normals of the desired neural SDF to avoid later iterations. We show below that both approaches can be made by mapping neural SDFs using nested neighborhoods.

The basic idea comes from the following fact: if the zero-level set of a neural SDF f is contained in a neighborhood V of the zero-level set of another neural SDF, then we can map f into V . This approach results in novel algorithms for sphere tracing, and normal mapping.

3.1. Overview

We focus on a simple example with three SDFs as an overview. We follow the notation in Fig. 1. Let S_1, S_2, S_3 be surfaces pairwise close. We assume their SDFs f_1, f_2, f_3 to be sorted by complexity, so evaluating f_1 is easier than f_2 and f_3 . We use S_1 and S_2 to illustrate the multiscale ST and S_3 to illustrate the neural normal mapping.

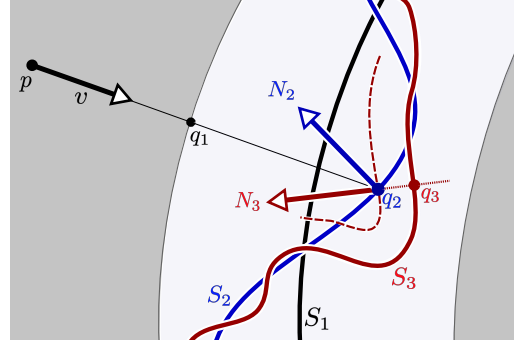


Figure 1. Overview. Let S_1, S_2, S_3 be a sequence of surfaces pairwise close. *Multiscale ST*: to sphere trace S_2 we first sphere trace the boundary of a neighborhood of S_1 (gray), resulting in q_1 . Then we continue to sphere trace S_2 , reaching q_2 . *Neural normal mapping*: since q_2 belongs to a (tubular) neighborhood of S_3 , we evaluate the normal N_3 at q_2 of a parallel surface of S_3 (red dotted). Notice that these surfaces share the same normal field.

Multiscale ST

Suppose that the ray $p + tv$, with origin at a point p and direction v , intersects S_2 at a point q_2 . To compute q_2 , we first sphere trace the boundary of a neighborhood of S_1 (gray) containing S_2 , by using f_1 . This results in q_1 . Then we continue to sphere trace S_2 using f_2 , reaching q_2 . In other words, we are mapping the values of f_2 to the neighborhood of S_1 . Using an inductive argument allows us to extend this idea to a sequence of SDFs. See Sec. 3.2 for details.

Neural Normal Mapping

For shading purposes, we need a normal vector at q_2 . This can be achieved by evaluating the gradient $N_2 = \nabla f_2(q_2)$ of f_2 at q_2 . Instead, we propose to pull the finer details of S_3 to S_2 to increase fidelity. This is done by mapping the normals from S_3 to S_2 using $N_3 = \nabla f_3(q_2)$.

To justify this choice observe that q_2 belongs to a (tubular) neighborhood of S_3 . Thus, N_3 is the normal of S_3 at its closest point $q_3 = q_2 - \epsilon N_3$, where ϵ is the distance from q_2 to S_3 given by $f_3(q_2)$. Thus, we are transferring the normal N_3 of S_3 at q_3 to q_2 . Observe that N_3 is also the normal of the ϵ -level set of f_3 at q_2 (red dotted).

3.2. Definition

A *neural SDF* $f_\theta : \mathbb{R}^3 \rightarrow \mathbb{R}$ is a smooth neural network with parameters θ such that $|\nabla f_\theta| \approx 1$. We call its *zero-level set* a *neural surface* and denote it by S_θ .

Let $f_{\theta_1}, f_{\theta_2}$ be neural SDFs. We say that f_{θ_2} is *nested* in f_{θ_1} for thresholds $\delta_1, \delta_2 > 0$ if the δ_2 -neighborhood of S_{θ_2} is contained in the δ_1 -neighborhood of S_{θ_1} :

$$[|f_{\theta_2}| \leq \delta_2] \subset [|f_{\theta_1}| \leq \delta_1]. \quad (1)$$

For simplicity, we denote it by $f_{\theta_1} \triangleright f_{\theta_2}$ and omit the thresholds δ_i in the notation. See Sec. 3.3 for examples.

A sequence of neural SDFs $f_{\theta_1}, \dots, f_{\theta_m}$ is *nested* if $f_{\theta_j} \triangleright f_{\theta_{j+1}}$ for $j = 1, \dots, m-1$. We use S_j to denote their neural surfaces. The nesting condition implies that each neural surface S_{j+1} is contained in $[|f_{\theta_j}| \leq \delta_j]$. Thus, to sphere trace S_{j+1} we can first sphere trace the δ_j -level set $S_j + \delta_j$ of f_{θ_j} , then continue using $f_{\theta_{j+1}}$ (see Fig. 2).

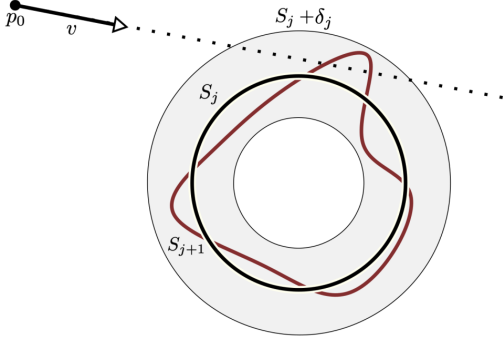


Figure 2. Illustration of a ray intersecting a pair of neural surfaces S_j and S_{j+1} with their neural SDFs satisfying $f_{\theta_j} \triangleright f_{\theta_{j+1}}$.

We can also extend these sequences to support animation by using 4D 1-families of neural SDFs. For this, suppose that the underlying sequence of networks $f_{\theta_1}, \dots, f_{\theta_m}$ has the *space-time* $\mathbb{R}^3 \times \mathbb{R}$ as domain. Then, we require the sequence of neural SDFs $f_{\theta_1}(\cdot, t) \triangleright \dots \triangleright f_{\theta_m}(\cdot, t)$ to be nested, for each t . See [1] for more details on families of neural SDFs. Varying t animates $f_{\theta_1}(\cdot, 0) \triangleright \dots \triangleright f_{\theta_m}(\cdot, 0)$.

3.3. Nesting the Neighborhoods

In this Section, we describe theoretical and practical approaches to create sequences of neural SDFs with nested neighborhoods. The objective is to train a sequence of neural SDFs sorted by inference time and to find small upper-bound thresholds that ensure the nesting condition. The supplementary material presents the proofs of the propositions in this Section.

BACON

Since BACON [17] is a multiresolution network to represent neural SDFs, its levels of detail are naturally sorted by

inference time and can be used to define our neural SDF sequence. Specifically, let $f_{\theta_j} : \mathbb{R}^3 \rightarrow \mathbb{R}$ be m LODs of a BACON network, and $\epsilon > 0$ be a small number. Defining $\varepsilon_j := |f_{\theta_j} - f_{\theta_{j-1}}|_\infty + \epsilon$ results in $|f_{\theta_j} - f_{\theta_{j-1}}|_\infty < \varepsilon_j$; where $|f|_\infty = \sup \{|f(p)|; p \in \mathbb{R}^3\}$. Then, Proposition 1 gives the thresholds δ_i implying that f_{θ_j} satisfy the nesting condition, i.e. $f_{\theta_1} \triangleright \dots \triangleright f_{\theta_m}$.

Prop. 1 Let f_i be m functions satisfying $|f_i - f_{i-1}|_\infty < \varepsilon_i$ for $\varepsilon_i > 0$. This sequence is nested for the thresholds δ_i defined by $\delta_m = \varepsilon_m$ and $\delta_{i-1} := \delta_i + \varepsilon_i$ for $i = 2, \dots, m$.

MLPs for a single surface

MLPs tend to learn lower frequencies first, a phenomenon known as the *spectral bias* [24]. Thus, we propose training MLPs with increasing capacity to represent a single SDF, resulting in a sequence of neural SDFs sorted by inference time and also by detail representation capacity. We use the approach presented in [22] to train each neural SDF.

Specifically, let S be a surface, and f be its SDF. Consider $f_{\theta_j} : \mathbb{R}^3 \rightarrow \mathbb{R}$ to be m MLPs approximating f sorted by capacity, i.e., there are small numbers $\varepsilon_j > 0$ such that $|f - f_{\theta_j}|_\infty < \varepsilon_j$. Thus, Proposition 2 gives the thresholds $\delta_i > 0$ which result in $f_{\theta_1} \triangleright \dots \triangleright f_{\theta_m}$.

Prop. 2 Let f be a function and f_{θ_i} be neural SDFs such that $|f - f_{\theta_i}|_\infty < \varepsilon_i$, where $\varepsilon_i > 0$. f_{θ_i} satisfy the nested condition for the thresholds δ_i defined by $\delta_m = \varepsilon_m + \varepsilon_{m-1}$ and $\delta_{i-1} := \delta_i + \varepsilon_i + \varepsilon_{i-1}$ for $i = 2, \dots, m$.

To compute the thresholds δ_j we need to evaluate the infinity norm $|f|_\infty$ of the underlying network f on its training domain. In practice, we approximate it by $\max \{|f(p_i)|\}$, where p_i are points sampled from the domain.

MLPs for multiple surfaces

This is a theoretical result that relates surfaces in *level of detail* with the existence of nested sequences of neural SDFs.

Let S_1, \dots, S_m be surfaces in level of detail such that S_j deviates no more than a small number $\varepsilon_j > 0$ from S_{j-1} . That is, $d(S_{i-1}, S_i) < \varepsilon_i$, where d is the *Hausdorff distance*. Such sequences of surfaces are considered by [10] in the context of meshes. Let $\epsilon > 0$ be a small number. The *universal approximation theorem* [7] states that there are MLPs f_{θ_j} that deviates no more than ϵ from the SDFs f_j of S_j . Prop. 3 provides the thresholds δ_i that imply $f_{\theta_1} \triangleright \dots \triangleright f_{\theta_m}$.

Prop. 3 Let S_i be m surfaces such that $d(S_{i-1}, S_i) < \varepsilon_i$, with $\varepsilon_i > 0$. For any $\epsilon > 0$, there are neural SDFs approximating the SDFs of S_i that are nested for the thresholds defined by $\delta_m = \epsilon$ and $\delta_{i-1} = \delta_i + \varepsilon_i + 2\epsilon$ for $1 < i \leq m$.

4. Multiscale Sphere Tracing

Let $f_{\theta_1} \triangleright \dots \triangleright f_{\theta_m}$ be a nested sequence of neural SDFs, p be a point outside $[|f_{\theta_1}| \leq \delta_1]$, and v be a direction. We define a multiscale ST that approximates the first hit between the ray $\gamma(t) = p + tv$, with $t > 0$, and the neural surface S_m (see Alg. 1). It is based on the fact that to sphere trace S_{j+1} we can first sphere trace $S_j + \delta_j$ using f_{θ_j} (see Fig. 2). Then we continue to iterate in $[|f_{\theta_j}| \leq \delta_j]$ using $f_{\theta_{j+1}}$. Lines 3-6 describe the sphere tracing of $S_j + \delta_j$ for $j = 1, \dots, m$ (line 1). If $j = m$ we sphere trace the desired surface S_m instead of its neighborhood (line 4).

In the dynamic case, the algorithm operates in 1-families of nested neural SDFs indexed by the time parameter.

ALGORITHM 1: Multiscale ST

Input: A sequence $f_{\theta_1} \triangleright \dots \triangleright f_{\theta_m}$, position p , unit direction v , and a threshold $\epsilon > 0$.
Output: End point p

```

1 for  $j = 1, \dots, m$  do
2    $t = +\infty$ ;
3   while  $t > \epsilon$  do
4      $t = (j=m) ? f_{\theta_j}(p) : f_{\theta_j}(p) - \delta_j$ ;
5      $p = p + tv$ ;
6   end
7 end
```

If $\gamma \cap S_m \neq \emptyset$, we can prove that the multiscale ST approximates the first hit point q between the ray γ and S_m . Indeed, by the nesting condition, if $\gamma \cap (S_j + \delta_j) \neq \emptyset$ implies $\gamma \cap (S_{j-1} + \delta_{j-1}) \neq \emptyset$. The classical ST guarantees that iterating $p = p + f_{\theta_j}(p)v$ approximates the intersection between γ and $S_j + \delta_j$. The proof follows by induction.

For the inference of a neural SDF, in line 4 of Alg. 1, we use the GEMM alg. [9] for each layer. The final step for rendering is to calculate the normals, given by the gradients of a detailed neural SDF. The next section describes the process.

5. Neural Normal Mapping

We propose an analytical computation of normals and a neural normal mapping procedure, which are decoupled from the multiscale ST. Those approaches are continuous, avoiding the need of specific methods to handle discretization, such as *finite differences*. This results in smooth normals, as shown in Figure 3.

The idea is to use a finer neural SDF f_θ to provide the normals of a coarse surface S nested in a δ -neighborhood of the zero-level set S_θ , i.e. $S \subset [|f_\theta| \leq \delta]$. The *neural normal mapping* assigns to each point p in S the normal $N_\theta(p) := \nabla f_\theta(p)$. This mapping is a restriction of ∇f_θ to the surface S . If ∇f_θ have no critical points in $[|f_\theta| \leq \delta]$, each point $p \in S$ can be connected to a point $q \in S_\theta$ by

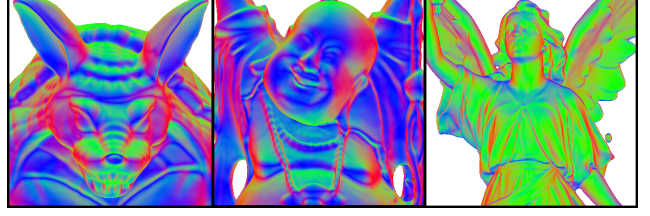


Figure 3. Rendering of the normals calculated using our framework. They are naturally smooth as a consequence of working on the continuous setting.

integrating the vector field $-\nabla f_\theta$. Thus, the neural normal mapping transports the normal $\nabla f_\theta(q)$ of S_θ , along the resulting path, to the point p by using $\nabla f_\theta(p)$. If $|\nabla f_\theta| = 1$ this path is a straight line and the vector field is constant along it, implying in $\nabla f_\theta(q) = \nabla f_\theta(p)$ (See Fig. 1).

In practice, we cannot guarantee that ∇f_θ has no critical points in $[|f_\theta| \leq \delta]$. However, in our shading experiments, this is not a problem because the set of critical points of SDFs has a zero measure.

We explore two examples. First, consider S being a triangle mesh. In this case, the neural normal mapping transfers the detailed normals of the level sets of f_θ to the vertices of S . This approach is analogous to the classic normal mapping, which maps detailed normals stored in textures to meshes via parametrizations. However, our method is volumetric, automatic, and does not need such parametrizations. See Fig. 5.

For the second example, consider S to be the zero-level set of another coarse neural SDF. In this case, we can use the neural normal mapping to avoid the overhead of additional ST iterations. See Fig. 4. Animated neural SDFs are also supported by mapping the normals of $f_\theta(\cdot, t)$ into the animated surface.

5.1. Analytic Normal Calculation for MLPs

We present an algorithm based on GEMMs to analytically compute normals for MLP-based neural SDFs, designed for real-time applications. For this, remember that a MLP f_θ with $n - 1$ hidden layers has the following form:

$$f_\theta(p) = W_n \circ f_{n-1} \circ f_{n-2} \circ \dots \circ f_0(p) + b_n, \quad (2)$$

where $f_i(p_i) = \varphi(W_i p_i + b_i)$ is the i -layer. The smooth *activation function* φ is applied on each coordinate of the linear map $W_i : \mathbb{R}^{N_i} \rightarrow \mathbb{R}^{N_{i+1}}$ translated by $b_i \in \mathbb{R}^{N_{i+1}}$.

We compute the gradient of f_θ using the *chain rule*

$$\nabla f_\theta(p) = W_n \cdot \mathbf{J} f_{n-1}(p_{n-1}) \cdot \dots \cdot \mathbf{J} f_0(p). \quad (3)$$

\mathbf{J} is the *Jacobian* and $p_i := f_{i-1} \circ \dots \circ f_0(p)$. The Jacobians of f_i applied to the points p_i are given by [22]:

$$\mathbf{J} f_i(p_i) = W_i \odot \varphi' [a_i | \dots | a_i] \quad (4)$$

where \odot is the *Hadamard* product, and the matrix $[a_i | \dots | a_i]$ has N_i copies of the vector $a_i = W_i(p_i) + b_i$.

The normals of S_θ are given by ∇f_θ which is a sequence of matrix multiplications (Eq 3). These multiplications do not fit into a GEMM setting directly since $\mathbf{J}f_0(p) \in \mathbb{R}^{3 \times N_1}$. This is a problem because the GEMM algorithm organizes the input points into a matrix, where its lines correspond to the point coordinates and its columns organize the points and enable parallelism. However, we can solve this problem using three GEMMs, one for each normal coordinate. Thus, each GEMM starts with a column of $\mathbf{J}f_0(p)$, eliminating one of the dimensions. The resulting multiplications can be asynchronous since they are completely independent.

The j -coord of $\nabla f_\theta(p)$ is given by $G_n = W_n \cdot G_{n-1}$, where G_{n-1} is obtained by iterating $G_i = \mathbf{J}f_i(p_i) \cdot G_{i-1}$, with the initial condition $G_0 = W_0[j] \odot \varphi'(a_0)$. The vector $W_0[j]$ denotes the j -column of the weight matrix W_0 .

We use a kernel and a GEMM to compute G_0 and G_n . For G_i with $0 < i < n$, observe that

$$G_i = (W_i \odot \varphi' [a_i | \dots | a_i]) \cdot G_{i-1} = (W_i \cdot G_{i-1}) \odot \varphi'(a_i).$$

The first equality comes from Eq. 4 and the second from a kind of commutative property of the Hadamard product. The second expression needs fewer computations and is solved using a GEMM followed by a kernel.

Alg. 2 presents the above gradient computation for a batch of points. The input is a matrix $P \in \mathbb{R}^{3 \times k}$ with columns storing the k points generated by the GEMM version of Alg. 1. The algorithm outputs a matrix $\nabla f_\theta(P) \in \mathbb{R}^{3 \times k}$, where its j -column is the gradient of f_θ evaluated at $P[j]$. Lines 2 – 5 are responsible for computing G_0 , lines 6 – 11 compute G_{n-1} , and line 13 provides the result G_n .

ALGORITHM 2: Normal computation

Input: neural SDF f_θ , positions P
Output: Gradients $\nabla f_\theta(P)$

```

1 for  $j = 0$  to 2 (async) do
2   using a GEMM: // Input Layer
3    $A_0 = W_0 \cdot P + b_0$ 
4   using a kernel:
5    $G_0 = W_0[j] \odot \varphi'(A_0)$ ;  $P_0 = \varphi(A_0)$ 
   // Hidden layers
6   for layer  $i = 1$  to  $n - 1$  do
7     using GEMMs:
8      $A_i = W_i \cdot P_{i-1} + b_i$ ;  $G_i = W_i \cdot G_{i-1}$ 
9     using a kernel:
10     $G_i = G_i \odot \varphi'(A_i)$ ;  $P_i = \varphi(A_i)$ 
11  end
12  using a GEMM: // Output layer
13   $G_n = W_n \cdot G_{n-1}$ 
14 end
```

6. Experiments

We present perceptual/quantitative experiments to evaluate our method. We fix the number of iterations for better control of parallelism. All experiments are conducted on an NVidia Geforce RTX 3090, with all pixels being evaluated (no acceleration structures are used).

We use a simplified notation to refer to the MLP architectures used. For example, $(64, 1) \triangleright (256, 3)$ means a neural SDF sequence with a MLP with one 64×64 matrix (2 hidden layers with 64 neurons), and a MLP with three 256×256 matrices (4 hidden layers with 256 neurons). Another example: $(64, 1)$ is a single MLP.

First, we discuss the two applications of neural normal mapping. Regarding image quality/perception, Figs. 4 and 5 show the case where the coarse surface is the zero-level of a neural SDF and when it is a triangle mesh, respectively. An overall evaluation of the framework is presented in Fig. 8. In all cases, normal mapping increases fidelity considerably.



Figure 4. Neural Normal Mapping into a neural SDF surface. On the left, a $(64, 1)$ neural SDF without normals mapped. On the right, a neural normal mapping of the $(256, 3)$ neural SDF into the $(64, 1)$.

The quantitative results corroborate the statement above. Table 1 shows performance metrics regarding time, memory, and mean square error (MSE) measured in a Python renderer. An important remark is that the neural normal mapping increases fidelity (up to 30% MSE improvement in comparison with the Armadillo coarse case) and considerably accelerates the rendering as well (up to 6x improvement in comparison with the Armadillo baseline).



Figure 5. Neural normal mapping into a triangle mesh surface. On the left side, the normals of a neural SDF (256, 3) are mapped into a coarse surface. On the right side, the original normals are used. The underlying surface is the same for both cases (marching cubes of a (64, 1) neural SDF). The MSE is 0.00262 for the coarse case and 0.00087 for the normal mapping, an improvement of 3x. The baseline is the marching cubes of the (256, 3) neural SDF.

The result may be improved using the multiscale ST, as shown in Figure 6. Adding ST iterations using a neural SDF with a better approximation of the surface improves the silhouette. This is aligned with the results presented in Table 1. The last two rows of each example show cases with iterations in the second neural SDF, with considerable improvement in the MSE (up to 20x improvement in comparison with the pure neural normal mapping for Lucy).

Table 2 shows a comparison with BACON in a Python renderer. We use a BACON network with 8 layers, with output in layers 2 and 6. For fairness, we use the same layers as neural SDFs for our method. The interpretation is analogous to the one for Table 1. To compare with the SIREN case, please refer to the numbers in that table.

We evaluated a GPU version implemented in a CUDA renderer, using neural normal mapping, multiscale ST, and the analytical normal calculation (with GEMM implemented using CUTLASS). Table 3 shows the results. Notice that the framework achieves real-time performance and that using neural normal mapping and multiscale ST improves performance considerably.

Finally, Fig. 7 shows an evaluation of an animated neural SDF representing the interpolation of the Falcon and Witch models. The baseline neural SDF is (128, 2) and the coarse is (64, 1). The example normal mapping case runs in the CUDA renderer at 73FPS. See the supplementary video for

Table 1. Evaluation of our method considering two SIRENs in a Python renderer. Iters represent the number of iterations used in each one (0 means no iteration and thus pure neural normal mapping). Time is in seconds and memory is in KB. MSE is the mean square error compared with the baseline (in *italic*). We emphasize in bold how the neural normal mapping has minimal time impact and how increasing iterations on the second SDF improves MSE.

	Nets	Iters	Time	Mem	MSE
Armadillo	(256,3)	40	2.442	777	-
	(64,1)	40	0.298	18	0.00588
	(64,1) ▷ (256,3)	40,0	0.409	795	0.00452
	(256,3)	15	0.936	777	0.01237
	(64,1) ▷ (256,3)	30,10	0.895	795	0.00746
	(64,1) ▷ (256,3)	30,30	1.934	795	0.00057
Buddha	(256,3)	40	2.228	777	-
	(64,1)	40	0.299	18	0.00485
	(64,1) ▷ (256,3)	40,0	0.413	795	0.00441
	(256,3)	15	0.928	777	0.00589
	(64,1) ▷ (256,3)	30,10	0.893	795	0.00355
	(64,1) ▷ (256,3)	30,30	1.945	795	0.00048
Bunny	(256,3)	40	2.237	777	-
	(64,1)	40	0.287	18	0.00229
	(64,1) ▷ (256,3)	40,0	0.403	795	0.00191
	(256,3)	15	0.928	777	0.00793
	(64,1) ▷ (256,3)	30,10	0.886	795	0.00417
	(64,1) ▷ (256,3)	30,30	1.920	795	0.00065
Lucy	(256,3)	40	2.239	777	-
	(64,1)	40	0.312	18	0.00518
	(64,1) ▷ (256,3)	40,0	0.420	795	0.00470
	(256,3)	15	0.941	777	0.00280
	(64,1) ▷ (256,3)	30,10	0.927	795	0.00363
	(64,1) ▷ (256,3)	30,30	1.977	795	0.00024



Figure 6. Silhouette evaluation. Left: (64, 1) ▷ (256, 3), right: (64, 1) ▷ (256, 2) ▷ (256, 3). Notice how the silhouettes improve with the additional (256, 2) level.

Table 2. Comparison with BACON [17] in a Python renderer. We use a BACON network with 8 layers, with output in layers 2 and 6. For fairness, we use the same layers as SDFs for our method. This Table follows the same structure of Table 1.

	Nets	Iters	Time	Mem	MSE
Armadillo	(256,6)	100	10.067	2151	-
	(256,2)	100	4.829	2151	0.00473
	(256,2) \triangleright (256,6)	100,0	4.945	2151	0.00309
	(256,2) \triangleright (256,6)	50,30	5.526	2151	0.00061
	(256,2) \triangleright (256,6)	50,50	7.438	2151	0.00040
Buddha	(256,6)	100	9.851	2151	-
	(256,2)	100	4.836	2151	0.00455
	(256,2) \triangleright (256,6)	100,0	4.946	2151	0.00284
	(256,2) \triangleright (256,6)	50,30	5.520	2151	0.00086
	(256,2) \triangleright (256,6)	50,50	7.450	2151	0.00077
Bunny	(256,6)	100	9.861	2151	-
	(256,2)	100	4.835	2151	0.00458
	(256,2) \triangleright (256,6)	100,0	4.952	2151	0.00260
	(256,2) \triangleright (256,6)	50,30	5.524	2151	0.00025
	(256,2) \triangleright (256,6)	50,50	7.455	2151	0.00013
Lucy	(256,6)	100	9.871	2151	-
	(256,2)	100	4.852	2151	0.00400
	(256,2) \triangleright (256,6)	100,0	4.968	2151	0.00207
	(256,2) \triangleright (256,6)	50,30	5.559	2151	0.00023
	(256,2) \triangleright (256,6)	50,50	7.488	2151	0.00018

Table 3. Real-time evaluation using SIRENs with our analytical normal calculation in a CUDA renderer. The number of iterations is 20 for the first neural SDF and 5 for the second neural SDF in the last row. The last network is used for neural normal mapping only. All pixels are evaluated. Images are 512×512 . Memory is in KB. Notice that all cases using multiscale ST and neural normal mapping result in speedups.

Model	FPS	Speedup	Mem
(256,3)	19.8	1.0	777
(64,1)	128.8	6.5	18
(64,1) \triangleright (256,1)	73.1	3.7	281
(64,1) \triangleright (256,2)	53.0	2.7	538
(64,1) \triangleright (256,3)	41.6	2.1	795
(64,1) \triangleright (256,1) \triangleright (256,3)	39.1	2.0	1058

the full animation.

7. Conclusion

We presented a novel approach to render neural SDFs based on three decoupled algorithms: the multiscale ST, the neural normal mapping, and the analytic normal calculation for MLPs. Those algorithms support animated 3D models and do not need spatial data structures to work. Neural normal mapping can also be used on contexts outside neural SDFs, enabling smooth normal fetching for discretized representations such as meshes as well.

This work opens paths for several future work options.

For example, exploring the mapping for other attributes could be interesting. Possible candidates include material properties, BRDFs, textures, and hypertextures.

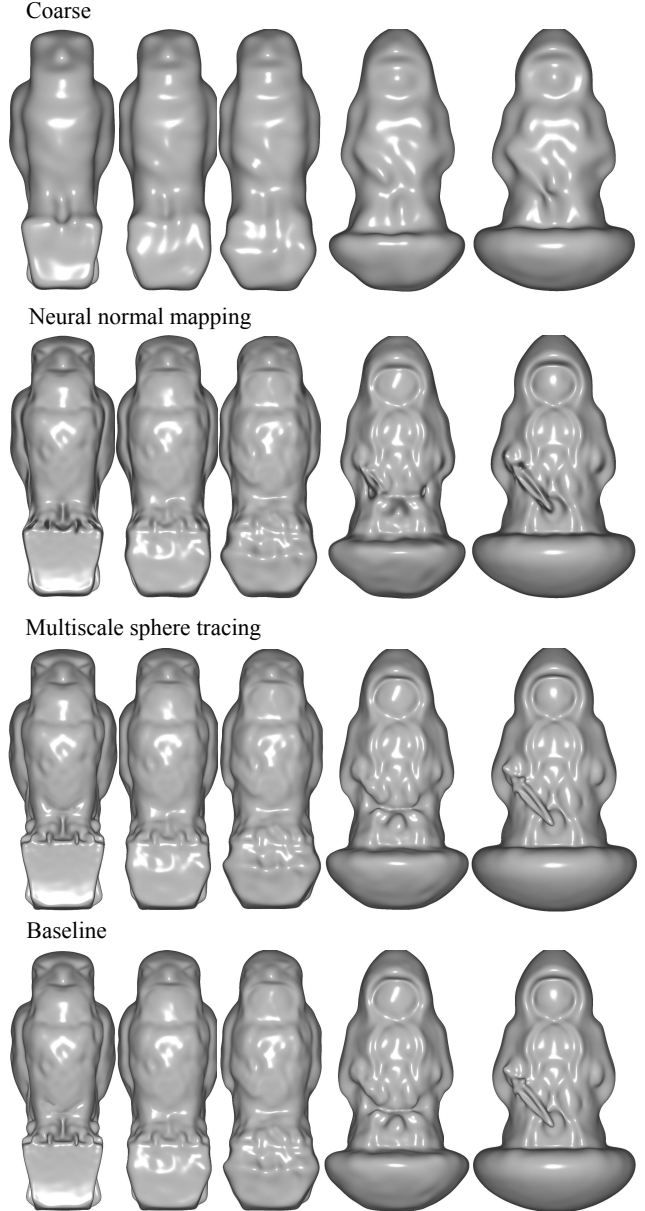


Figure 7. Interpolation between the Falcon and Witch models. From top to bottom: (64,1), (64,1) \triangleright (128,2), and the baseline (128,2). Notice how the normal mapping in the second line increases fidelity. See the video in the supplementary material.

Another path to explore is performance. Improvements can be done for further optimization. For example, using fully fused GEMMs may decrease the overhead of GEMM setup [21]. The framework may also be adapted for acceleration structures and ray tracing engines such as OptiX.

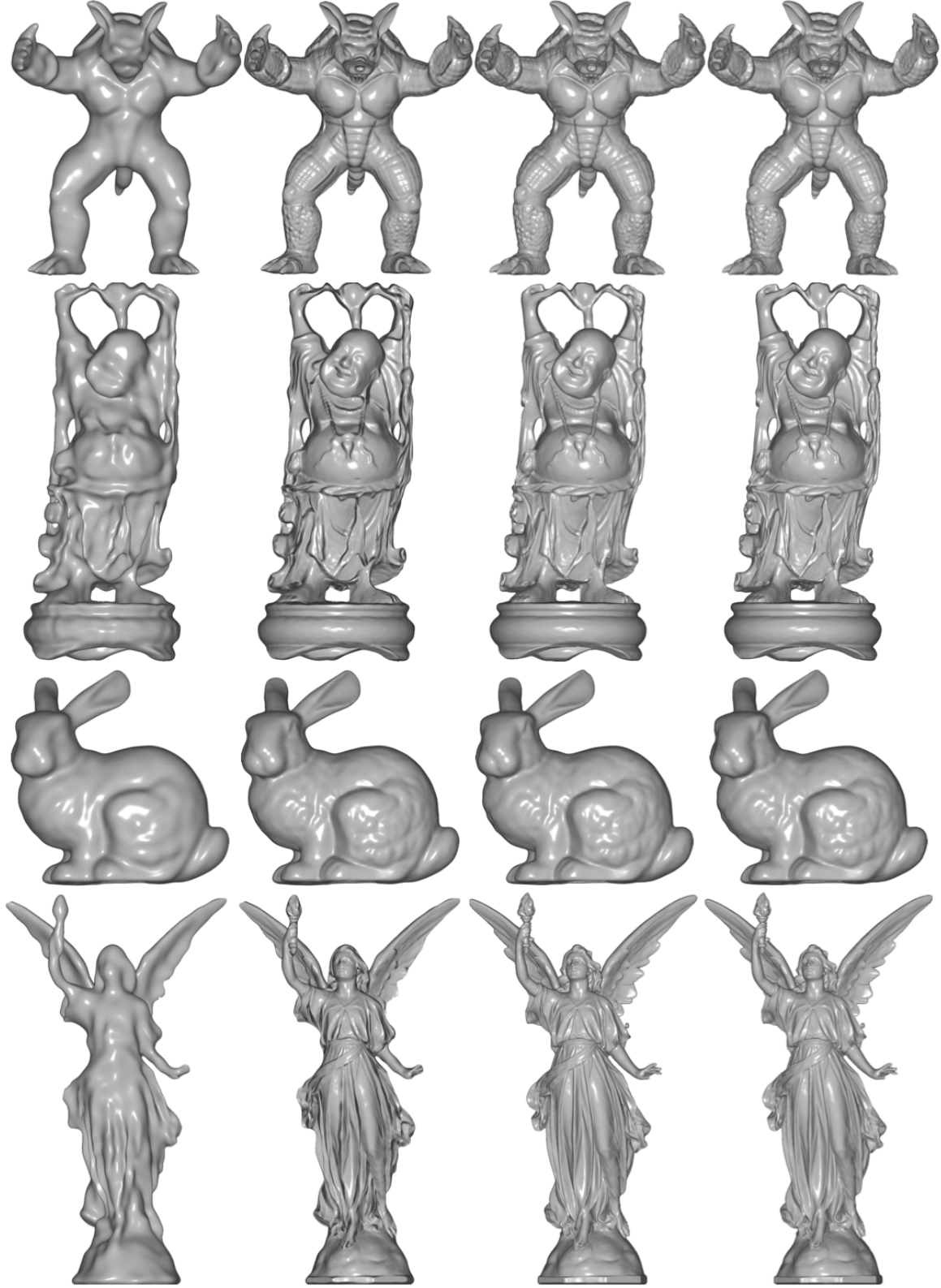


Figure 8. Comparison between our method and the SIREN baseline. The columns represent different configurations. From left to right: $(64, 1)$, $(64, 1) \triangleright (256, 1)$ (Bunny and Dragon) and $(64, 1) \triangleright (256, 2)$ (Happy Buddha and Lucy), $(64, 1) \triangleright (256, 3)$, and the baseline $(256, 3)$. Notice how the second column is already similar to the baseline. The third column adds more detail.

References

- [1] Anonymous. Neural implicit surface evolution using differential equations. 2022. [3](#)
- [2] J. F. Blinn. Simulation of wrinkled surfaces. *ACM SIGGRAPH computer graphics*, 12(3):286–292, 1978. [2](#)
- [3] J. Bloomenthal and B. Wyvill. Interactive techniques for implicit modeling. *ACM Siggraph Computer Graphics*, 24(2): 109–116, 1990. [1](#)
- [4] Z. Chen and H. Zhang. Neural marching cubes. *ACM Trans. Graph.*, 40(6), dec 2021. ISSN 0730-0301. doi: 10.1145/3478513.3480518. URL <https://doi.org/10.1145/3478513.3480518>. [2](#)
- [5] P. Cignoni, C. Montani, C. Rocchini, and R. Scopigno. A general method for preserving attribute values on simplified meshes. In *Proceedings Visualization'98 (Cat. No. 98CB36276)*, pages 59–66. IEEE, 1998. [2](#)
- [6] J. Cohen, M. Olano, and D. Manocha. Appearance-preserving simplification. In *Proceedings of the 25th annual conference on Computer graphics and interactive techniques*, pages 115–122, 1998. [2](#)
- [7] G. Cybenko. Approximation by superpositions of a sigmoidal function. *Mathematics of control, signals and systems*, 2(4):303–314, 1989. [3](#)
- [8] T. Davies, D. Nowrouzezahrai, and A. Jacobson. On the Effectiveness of Weight-Encoded Neural Implicit 3D Shapes. 2020. URL <http://arxiv.org/abs/2009.09808>. [2](#)
- [9] J. J. Dongarra, J. Du Croz, S. Hammarling, and I. S. Duff. A set of level 3 basic linear algebra subprograms. *ACM Transactions on Mathematical Software (TOMS)*, 16(1):1–17, 1990. [2, 4](#)
- [10] M. Eck, T. DeRose, T. Duchamp, H. Hoppe, M. Lounsbery, and W. Stuetzle. Multiresolution analysis of arbitrary meshes. In *Proceedings of the 22nd annual conference on Computer graphics and interactive techniques*, pages 173–182, 1995. [3](#)
- [11] A. Gropp, L. Yariv, N. Haim, M. Atzmon, and Y. Lipman. Implicit geometric regularization for learning shapes. *arXiv preprint arXiv:2002.10099*, 2020. [1, 2](#)
- [12] J. C. Hart. Sphere tracing: A geometric method for the antialiased ray tracing of implicit surfaces. *The Visual Computer*, 12(10):527–545, 1996. [1, 2](#)
- [13] J. C. Hart, D. J. Sandin, and L. H. Kauffman. Ray tracing deterministic 3-D fractals. In *Proceedings of the 16th Annual Conference on Computer Graphics and Interactive Techniques*, pages 289–296, 1989. [1, 2](#)
- [14] V. Krishnamurthy and M. Levoy. Fitting smooth surfaces to dense polygon meshes. In *Proceedings of the 23rd annual conference on Computer graphics and interactive techniques*, pages 313–324, 1996. [2](#)
- [15] T. Lewiner, H. Lopes, A. W. Vieira, and G. Tavares. Efficient implementation of marching cubes’ cases with topological guarantees. *Journal of graphics tools*, 8(2):1–15, 2003. [2](#)
- [16] Y. Liao, S. Donne, and A. Geiger. Deep marching cubes: Learning explicit surface representations. In *Proceedings of CVPR*, pages 2916–2925, 2018. [2](#)
- [17] D. B. Lindell, D. Van Veen, J. J. Park, and G. Wetzstein. BACON: Band-limited Coordinate Networks for Multiscale Scene Representation. 2021. URL <http://arxiv.org/abs/2112.04645>. [2, 3, 7](#)
- [18] S. Liu, Y. Zhang, S. Peng, B. Shi, M. Pollefeys, and Z. Cui. Dist: Rendering deep implicit signed distance function with differentiable sphere tracing. In *Proceedings of CVPR*, pages 2019–2028, 2020. [2](#)
- [19] W. E. Lorensen and H. E. Cline. Marching cubes: A high resolution 3d surface construction algorithm. *ACM siggraph computer graphics*, 21(4):163–169, 1987. [2](#)
- [20] J. N. P. Martel, D. B. Lindell, C. Z. Lin, E. R. Chan, M. Monteiro, and G. Wetzstein. ACORN: Adaptive Coordinate Networks for Neural Scene Representation. *ACM Transactions on Graphics*, 40(4):1–13, may 2021. ISSN 0730-0301. doi: 10.1145/3450626.3459785. URL <https://dl.acm.org/doi/10.1145/3450626.3459785> <http://arxiv.org/abs/2105.02788>. [2](#)
- [21] T. Müller. Tiny CUDA neural network framework, 2021. <https://github.com/nvmlabs/tiny-cuda-nn>. [2, 7](#)
- [22] T. Novello, G. Schardong, L. Schirmer, V. da Silva, H. Lopes, and L. Velho. Exploring differential geometry in neural implicits. *Computers & Graphics*, 108, 2022. ISSN 0097-8493. doi: <https://doi.org/10.1016/j.cag.2022.09.003>. URL https://dsilvavinicius.github.io/differential_geometry_in_neural_implicits/. [1, 2, 3, 4](#)
- [23] J. J. Park, P. Florence, J. Straub, R. Newcombe, and S. Lovegrove. Deepsdf: Learning continuous signed distance functions for shape representation. In *Proceedings of CVPR*, pages 165–174, 2019. [1, 2](#)
- [24] N. Rahaman, A. Baratin, D. Arpit, F. Draxler, M. Lin, F. Hamprecht, Y. Bengio, and A. Courville. On the spectral bias of neural networks. In *International Conference on Machine Learning*, pages 5301–5310. PMLR, 2019. [3](#)
- [25] J. A. Sethian and A. Vladimirsky. Fast methods for the eikonal and related hamilton-jacobi equations on unstructured meshes. *Proceedings of the National Academy of Sciences*, 97(11):5699–5703, 2000. [1](#)
- [26] V. Sitzmann, J. Martel, A. Bergman, D. Lindell, and G. Wetzstein. Implicit neural representations with periodic activation functions. *Advances in Neural Information Processing Systems*, 33, 2020. [1, 2](#)
- [27] T. Takikawa, J. Litalien, K. Yin, K. Kreis, C. Loop, D. Nowrouzezahrai, A. Jacobson, M. McGuire, and S. Fidler. Neural Geometric Level of Detail: Real-time Rendering with Implicit 3D Shapes. pages 11353–11362. IEEE, jun 2021. ISBN 978-1-6654-4509-2. doi: 10.1109/CVPR46437.2021.01120. URL <https://ieeexplore.ieee.org/document/9578205/>. [2](#)
- [28] L. Velho, J. Gomes, and L. H. de Figueiredo. *Implicit objects in computer graphics*. Springer Science & Business Media, 2007. [1](#)